Research Square

Preprints are preliminary reports that have not undergone peer review.
They should not be considered conclusive, used to inform clinical practice,
or referenced by the media as validated information.

Tribology and corrosion behavior of Gray Cast Iron brake discs coated with Inconel 718 by Direct Energy Deposition

Diana CHIOIBASU (diana.chioibasu@inflpr.ro)
National Institute for Laser Plasma and Radiation Physics: Institutul National de Fizica Laserilor Plasmei si Radiatiei https://orcid.org/0000-0003-3024-7744
Sabin MIHAI
Cosmin M. COTRUT
Ionelia VOICULESCU
Andrei C. POPESCU

Research Article

Keywords: Direct Energy Deposition, Brake discs, Inconel 718, Wear resistance, Corrosion behavior.

Posted Date: March 14th, 2022

DOI: https://doi.org/10.21203/rs.3.rs-1415771/v1

License: This work is licensed under a Creative Commons Attribution 4.0 International License.
Read Full License

Tribology and corrosion behavior of Gray Cast Iron brake discs coated with Inconel 718 by Direct Energy Deposition

Diana CHIOIBASU[1], Sabin MIHAI[1,3], Cosmin M. COTRUT[2], Ionelia VOICULESCU[2*], Andrei C. POPESCU[1*]

[1]Center for Advanced Laser Technologies, National Institute for Laser, Plasma and Radiation Physics (INFLPR), Ilfov, 077125 Magurele, Romania

[2]University Politehnica of Bucharest (UPB), Bucharest, 313 Splaiul Independentei, 060042 Bucharest Romania

[3]Faculty of Industrial Engineering and Robotics, University Politehnica of Bucharest, 060042 Bucharest, Romania

*andrei.popescu@inflpr.ro, ioneliav@yahoo.co.uk

Abstract

There has been an increased concern related to environmental pollution, caused by the emission of particles released during the braking process. In the future, environmental safety laws will be increasingly restrictive and the development of new viable alternative technologies will be inherent. Because gray cast iron (GCI) has a low cost and mechanical properties compatible with this type of application, it will be difficult to identify a similar material to replace it. In the case of vehicles that serve passenger transport, the most convenient solution is to cover the brake discs made of GCI with materials that reduce wear and corrosion, but which at the same time maintain or improve their functional performance. This research aims to improve the mechanical properties of the brake discs by laser cladding using Inconel 718 (IN718) metallic powder by Direct Energy Deposition (DED) method. The interface between substrate and the deposited material was uniform, forming a compact bonding of the two materials. The average hardness of the IN718 deposited material was twice higher than the one of the GCI substrates. The friction coefficient (CoF) of the IN718 coatings was higher by 0.12 compared with the substrate material. The depth of the wear track for the layers deposited with IN718 was -50 µm, while the depth of the wear track of the exposed substrate GCI was 3 times higher (-150 µm). The corrosion resistance of the coating was superior by four orders of magnitude to that of GCI substrate in 3.5 wt.% NaCl aqueous solution.

Keywords: Direct Energy Deposition; Brake discs; Inconel 718; Wear resistance; Corrosion behavior.

1. Introduction

Gray cast iron (GCI) is widely used in industry fields involving metallurgical processes due to its excellent physico-chemical properties (good casting behavior, superior conductivity, excellent thermal stability, high hardness and good abrasion resistance) which prevent overheating and surface wear, and it's low cost [1–3]. However, under severe usage circumstances, the wear performance, hardness and corrosion resistance of GCI can be drastically reduced. The coarse grains and inferior surface quality of GCI are the main disadvantages that impede on the widening of the possible applications and relatively reduced service life. An important application of GCI is the brake disc, which is an essential component of the braking system for automobile, aviation and rail vehicles. In the last decade, the environmental pollution caused by the emission of particles released during the braking process has attracted an increased attention and concern from environmental agencies, following proves from numerous studies and research efforts from all over the world [4–7] Due to the fact that GCI has mechanical properties compatible with this type of application, and the components made from it can be cast and machined at low cost, it will be difficult to identify a similar material to replace it. Aiming to overcome the above disadvantages, surface modification technology could be introduced to improve the performance of GCI. This can be the most suitable solution, as the brake discs made of GCI could be coated with materials for reducing wear and corrosion, while also succeeding to maintain or improve their functional performance [8].

The Fraunhofer Institute for Laser Technology ILT and RWTH Aachen University have developed an improved coating method using laser cladding as the basic technique, called "Extreme High-speed Laser Material Deposition (EHLA)". This technique seems to be extremely efficient in the process of coating brake discs with metallic layers with superior properties both from an economic and technical point of view, due to the use of high processing speeds (up to 8 m / s, compared to 0.008 -0.03 m/s) [9, 10].

Direct energy deposition (DED) is one of the numerous methods of coating metal surfaces with other metallic materials (air plasma spraying - APS, high-velocity oxygen fuel - HVOF, thermal spray, gas tungsten arc welding – GTAW, laser welding - LW, thermal barrier coatings - TBC) that can obtain excellent performance against wear and corrosion. DED is an additive manufacturing technology which allows coating in a single step of a layer with thickness dimensions between 0.3-2 mm. Such a layer made of metallic or composite materials possesses remarkable characteristics, such as reduced heat affected zone, minimal dilution and improves wear [11–14] and corrosion resistance [15–18]. DED can be found in literature as laser cladding (LC) or laser melting deposition (LMD) and has huge potential for refurbishing and transforming the surface of crucial components and expanding their service life [19]. However, the literature studies have shown that the DED technology applied to GCI materials has certain restrictions [20, 21] deposition of Co [22] and NiCrBSi [23] on GCI substrates has been studied using high power continuous emission laser sources, but cracks were observed in the structure of the deposited substrate. These defects were caused by the residual stresses that occur during the build of the deposited structure.

Inconel 718 (IN718) is a high-strength precipitation-hardening nickel-base alloy that has exceptional characteristics, including excellent mechanical properties in severe conditions, low creep at high temperatures, high oxidation resistance and hot corrosion resistance up to

650°C, as well as good welding behavior [16, 24, 25] Therefore, it is extensively used in various industries, such as petrochemical industries aerospace and marine.

When it comes to laser coating GCI, there are many problems to be solved: obtaining a good adhesion between the two materials due to the different chemical compositions and mechanical properties, reducing the dilution at the interface of the deposited layers, limiting the formation of Laves phases in order to reduce cracking and stress.

Stanciu & al. [26] deposited double layers of NiCrBSi and IN718 by laser-cladding on steel substrate. Thus, they obtained an increase in corrosion resistance, a reduction in dilution with the substrate, as well as a hardness gradient with increased values on the deposited NiCrBSi layer. Another study showed a successfully deposited NiCo coating on IN718 substrate by pulsed laser cladding. In this case, the hardness of the deposited layer was higher with 21% that the one of the IN718 substrate and the coating's surface residual stress was compressive stress, which prevents crack generation and improves fatigue strength [12]. Using a pulsed laser source, the heat affected area was smaller [27], cracks were reduced due to low heat input [28] and the hardness of the deposited layer increased with the use of a high pulse rate [29]. To eliminate the voids that occur during the laser cladding process on GCI a study about remelting of the deposited material was carried out. The results revealed that laser remelting was an effective way to eliminate the voids generated in the interface zone and microhardness of the hardened region was of ~ 600HV[30]. Another research investigated the effects of process parameters on the geometric characteristics, microstructure, and corrosion resistance of the Co-based coating on 42CrMo pipeline steel. The authors obtained excellent corrosion resistance through the adjustment of the process parameters [15]. The microstructure and tribological properties of the deposited layer were studied based on process parameters during laser cladding Ni-based on QT500-7 ductile cast iron. The hardness, corrosion resistance and tribological properties were significantly improved by optimizing the process. When the WC content is in 5%–35%, the microhardness increased 3 times. When the WC content is 20%, the corrosion current is three times lower that the one of the substrate which means that the corrosion resistance of the coating is higher. The wear rate of the substrate is almost seven times higher than the cladding layer with different WC mass fractions [31].

The effects of laser remelting speed of IN718 alloy layers obtained by LMD have been studied by Xin B. & all [32]. Using a high speed of LR process (3 times higher than the speed used in case of the LMD processing) the mean primary dendrite spacing values of the remelting area decreased from 6.35 to 3.28 μm gradually and the hardness increased with 12 HV. Mazzucatto & all [33] conducted a research study on the influence of LMD process parameters on the mechanical properties of IN718 depositions at room temperature and several deformation rates (i.e. 0.001, 200 and 800 / s) using a split Hopkinson drawbar. The results established an important influence of the LMD process parameters on the mechanical properties of the as-built metal compared to as-cast material and a good repeatability of the process. The influence of process parameters in case of the laser processing of cast iron in terms of dilution, layer width and heat affected zone were studied by Gusev & Lyukhter [34]. They developed a control scheme for the laser plating process to achieve a low level of dilution and to reduce the width of the heat affected zone. Liu & all [35] studied the effect of combined heat treatment (solid solution 1050ºC + double aging) on IN718 laser-coated layers. They showed that the hardness increased from 350HV to 500HV and the residual stress turned into compression stress after the heat treatment.

This paper focuses on an IN718 metallic coating of a GCI substrate, cut from a brake disc by DED technique, in which the filler material is supplied by a three-beam nozzle into the laser beam, obtaining after solidification an adherent, compact and uniform layer on the surface. We will show that the hardness tests, tribological tests and corrosion resistance showed higher values for the direct laser deposited layer compared to the base material. Functional braking tests on IN718 coated brake discs mounted on an autovehicle, performed by an official certification car service, showed that the friction values are in accordance with the brake discs specifications in the legislation for cars circulation in Romania.

2. Materials and methods

The metallic powder used for this study was nickel-based superalloy IN718 purchased from Hoganas GmbH (Germany, Goslar) with spherical shape particles and 45-90 μm diameter. Before experiments, the material was submitted to a thermal treatment at 60°C for 4h in furnace in order to eliminate the absorbed humidity from the atmosphere. The chemical composition of the powder material is listed in table 1.

Table 1. Chemical composition of IN718[wt%]

Ni %	Cr %	Nb %	Mo %	Ti %	Al %	Si %	Mn %	C %	Fe
52.8	19.2	5.29	3.1	1.0	0.6	<0.10	0.02	0.05	Balance

For this study, GCI samples obtained by cutting an automobile brake disc into 60 mm x 20 mm x 5 mm coupons were used as substrates. The typical microstructure of GCI is characterized by a dispersed carbon lamella formation surrounded by α-ferrite and pearlite phases. The chemical composition of the GCI substrate is listed in table 2. The substrate was machined by turning in order to remove surface debris and impurities and then cleaned with acetone and ethanol in order to completely remove the debris.

Table 2 Chemical composition of GCI [wt%]

C	Si	Mn	P	S	Cu	Fe
3.2-3.5	1.8-2.2	0.6-0.9	≤ 0.2	≤ 0.12	≤ 0.58	Balance

Physical and thermal properties of the GCI and IN718 such as specific heat capacity, coefficient of thermal expansion and thermal conductivity are presented in table 3.

Table 3. Physical and thermal properties of materials

Material	Density [kg/m^3]	Melting temperature [°C]	Thermal conductivity [W/m•K]	Caloric capacity [J/kg•K]	Thermal expansion coefficient [10^{-5}/K]
GCI	7090	1208	39	513	1.2
Inconel 718	8190	1260-1335	11.2	435	1.3

From the values of physical properties results that IN718 powder is compatible with the GCI in terms of crystalline structure, melting temperature and thermal expansion coefficient, while differences appear in case of the thermal conductivity. The powder type for laser cladding was chosen based on the criteria of compatibility with the main physical properties of hypoeutectic cast iron (carbon content between 2 and 4.11wt %, microstructure with uniform vermicular graphite spread in a mass of pearlite), in order to obtain the increase of the corrosion

resistance and of the coefficient of friction, without generating stress at the interface between the deposited material and the substrate.

The experimental set-up used for obtaining IN718 deposition layers by DED technique consists in a 3 kW Yb:YAG laser source (TruDisk 3001, Trumpf, Ditzingen, Germany) emitting in continuous mode, with wavelength λ=1030 nm connected by optical fiber to a deposition optics. The optics was mounted on a robotic arm (TruLaser Robot 5020, Trumpf, Ditzingen, Germany) with 8 degrees of freedom using an electro-magnetic plate.

The deposition line is equipped with a three-beam nozzle which ensures a uniform powder distribution, independent of the process motion (Fig. 1). The laser beam is guided and focused on the workpiece trough the focusing optics, while the powder stream is blown into the laser spot through 3 nozzles. The deposited layers were obtained by using 600 W laser power, 0.01 m/s scanning speed, 4 g/min powder debit and 14 slpm gas mix (He-Ar).

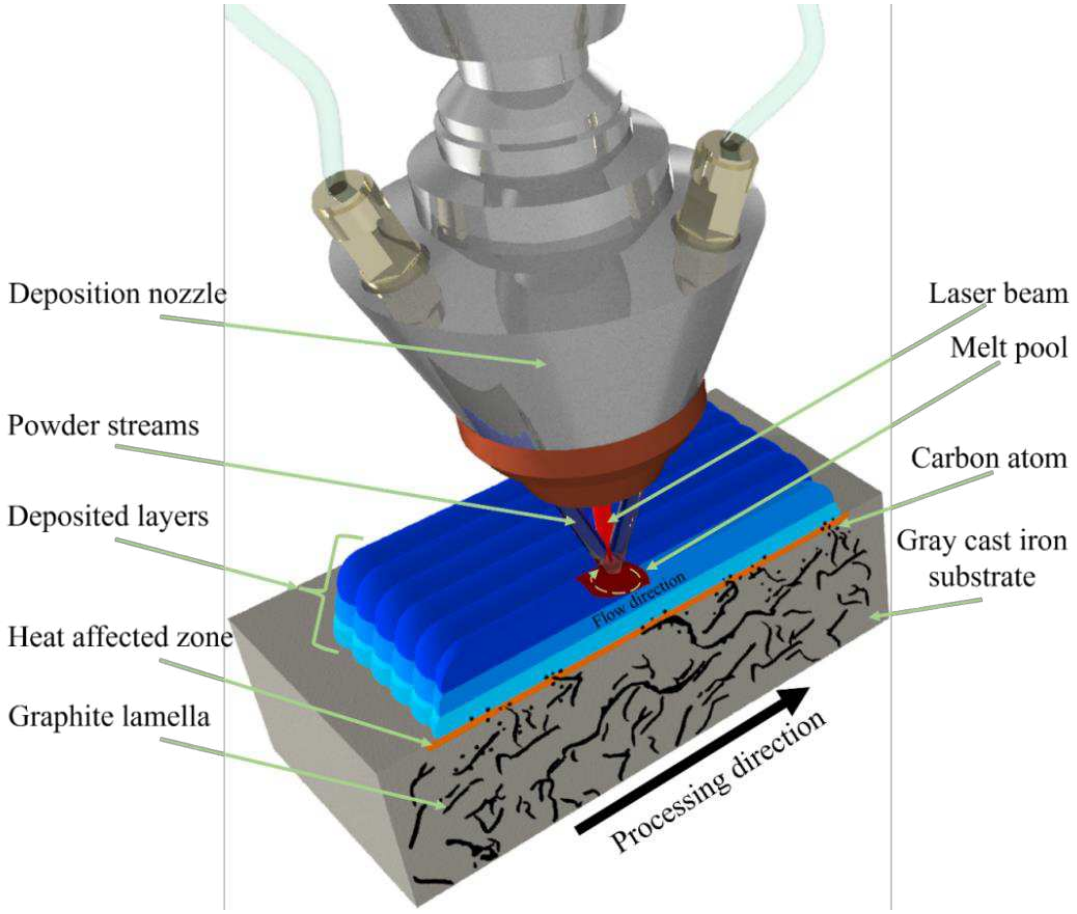

Fig. 1 Schematic representation of laser cladding and C atoms dynamics in the deposited layer

The laser beam (Ø=800 μm) was concentrated on the surface of the substrate via a 200 mm focal distance lens. The trajectory of the deposition layers was designed and programmed into the robot movement code generator, TruTops Cell® (Trumpf, Ditzingen, Germany) (Fig. 2a). The chosen scanning strategy used for laser cladding of the brake disc was a spiral like trajectory (Fig. 2b), to keep a low temperature during the process and to diminish the risk of C evaporation from the substrate as much as possible. In order to obtain a bulk structure, the optimum interspace distance of the spiral was found to be at 1 mm, while the distance between layers was of 0.2 mm, which translates in a 40% ratio overlap. Each layer deposited using these process parameters had a height of 600 μm.

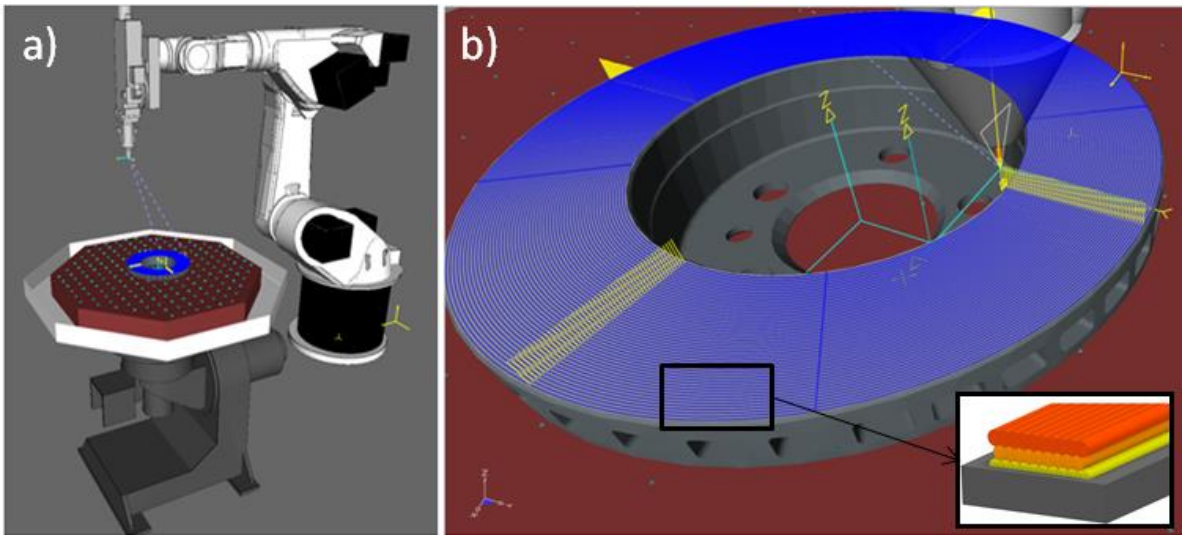

Fig. 2 Computer Aided Manufacturing program (a); Scanning strategy of the deposition with a superposed spirals detail (b)

The temperature of the molten pool was recorded by a non-contact pyrometer, IGA 5 (Fort Collins, Colorado) and the substrate temperature via a chromel-alumel thermocouple wire.

The deposited samples produced by DED technique on the GCI substrate were cut into small coupons of 10 mm × 10 mm × 10 mm by disc cutting method, which were used to analyze the microstructure, the hardness, the wear and corrosion resistance. The surfaces were mirror-like prepared to reveal the microstructure using silicon carbide sandpaper grinding (400 to 2500 grit paper), diamond abrasive paste polishing (3-0.1µm particle size), washed with running water, dried via cold air and then chemically etched using Kalling 2 reagent (ATM, Mammelzen, Germany). The geometrical characteristics of the cross section of the clad areas were analyzed and measured using an Olympus GX51 (Tokyo, Japan) optical microscope equipped with AnalySis software for images processing. The microstructure of cross sections through the laser clad samples were analyzed also by scanning electron microscopy (SEM) using Inspect S microscope (FEI, Holland) equipped with AMETEC Z2E EDS sensor.

The hardness was measured by scratch testing performed using a multi-function Tribometer MFT-2000 (Rtec-instruments, Yverdon-les-Bains, Switzerland) under constant load of 25N with 0.15 mm/s speed and a diamond Rockwell 200 µm radius on a 3 mm length at 23˚C temperature environment and 40% relative humidity. The scratch hardness number was calculated using equation 1, by dividing the applied normal force on the stylus by the projected area of scratching contact, considering the hemispherical - tipped stylus groove of a radius of curvature r. The projected area of the contact surface is therefore a semi-circle whose diameter is the final scratch width.

$$HS_P = \frac{8P}{\pi w^2} \tag{1}$$

where:

HS_P – scratch hardness number [GPa]; P – normal force [N]; w – scratch width [µm]

The same system was used for pin on disk tribological testing behavior under the following conditions: 60N applied load for 5 min, 150 rpm speed and a 6 mm diameter pin with spherical head made of Steel 440C. The testing machine is equipped with dedicated software for data analyses and interpretation. Prior measurements of the hardness and wear resistance on the IN718 deposited material and the GCI substrate, the surfaces were preliminary prepared by grinding and polishing.

The electrochemical measurements (corrosion tests) were carried out by using linear polarization resistance (LPR) technique, which is a corrosion rate monitoring method that can give an indication of the corrosion resistance of materials in an aqueous environment. The corrosion tests were carried out in a three-electrode cell using a PARSTAT 4000 (Princeton Applied Research - AMETEK, USA) potentiostat/galvanostat connected to the VersaStudio software produced by the same company. The measurements were conducted according ASTM G5 - 94(2011)e1 standard. The working electrode was made of the GCI without and with IN718 coating. The saturated calomel electrode (SCE) was used as the reference, and the recording electrode was made from a platinum mesh (99.8% Pt). Prior each measurement, the surface of the working electrode was cleaned ultrasonically in pure water and dried at room temperature. The used corrosive environment (electrolyte) was NaCl 3.5%. The potentiodynamic polarization (LSV) curves were recorded by applying a potential in range of −2000 to 2000 mV, with the scanning rate of 1 mV/s. The LSV curves were used to designate the corrosion potential, corrosion current density and the slope of the anodic and cathode curve of the tested materials. All measurements were carried out at a temperature of 24 ± 0.2 °C and to ensure repeatability, the tests were performed three times for each specimen.

3. Results and discussion

Microstructure

Both longitudinal and transversal cross sections through deposited layers were performed and the resulting surfaces were prepared for analyses. Figure 3a displays the optical microscopy image of a transversal cross-sectioned mirror-polished deposited layer of Inconel 718 on GCI substrate. Four cuts were performed in arbitrary places of the sample in order to check for the presence of defects. Tests were performed for determination of the optimal distance between two lines of deposited material, in order to obtain an esthetically pleasing, but also a defects free continuous deposition. A 40% overlap ratio between the meander lines when depositing the material was found to be the optimal value for achieving a homogenous, crack and pores-free surface in the alloyed region. This was consistent for all depositions on four studied samples. A typical cross-section is presented in Fig. 3b, showing a defects free bounding interface between the coatings and substrates. The deposited material thickness varies from 700 µm up to 900 µm for one layer deposition. Some detailed images from the interface between the IN718 deposition layers and the GCI support material are presented in figures 3c and 3d.

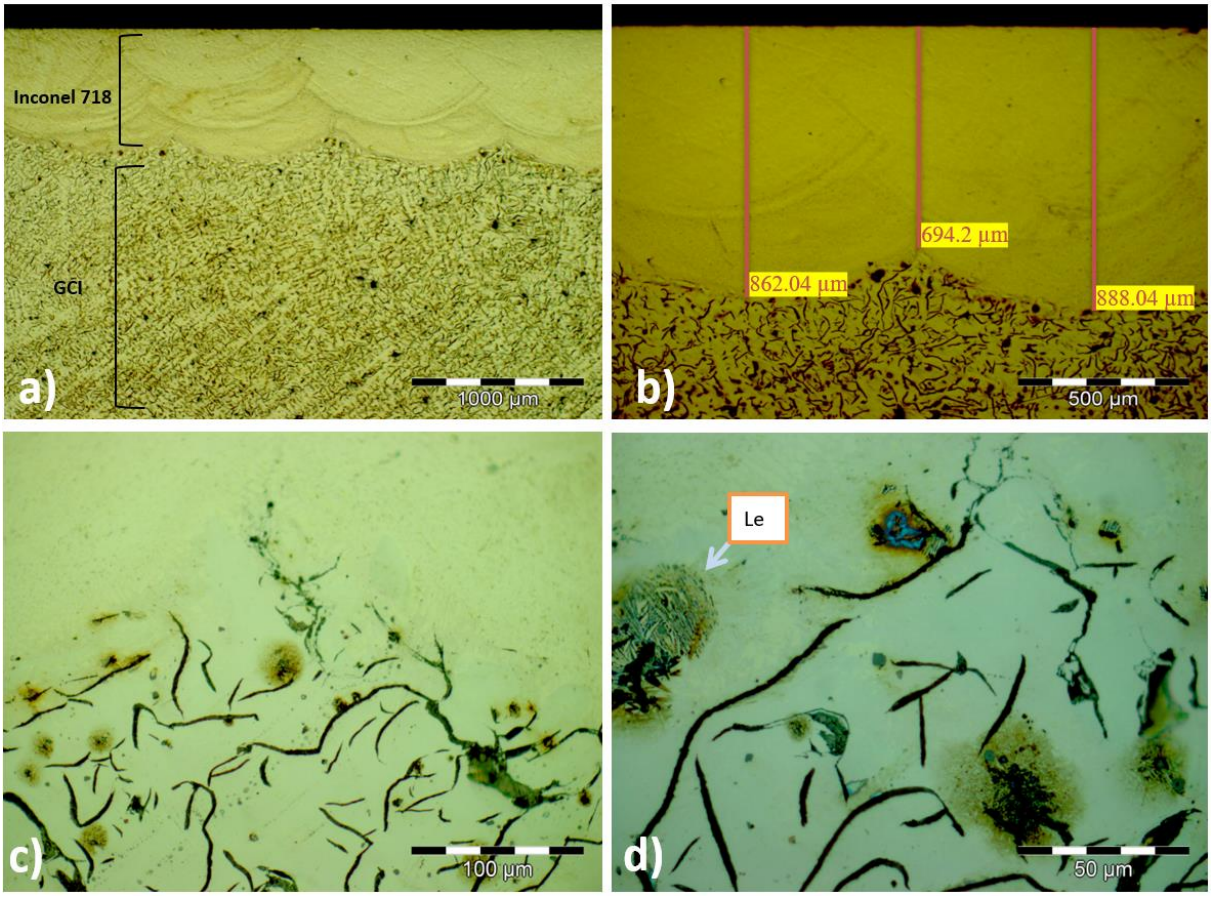

Fig. 3 Optical microscopy images of cross section of GCI substrate coated by DED with IN718 after the metallographic etching. Magnification bar: 1000 µm (a), 500 µm (b), 100 µm (c) and 50 µm (d).

It can be noticed that the graphite lamellae were deformed and coalesced at the interface between substrate and deposited material. In addition, small islands of Ledeburite (Le) were formed in the confluence zone between the deposited IN718 alloy and the GCI substrate. In the transversal cross section of laser deposition (Fig. 4a), the interface line is wavy, indicating the formation of mixing zones with the widths corresponding to each passing of the laser beam. In contrast, the interface with the GCI substrate in the longitudinal cross section is quite linear and has a narrow mixing zone (MZ). The structure in the laser deposition area shows a cellular dendritic growth (Fig. 4b), oriented in the direction of heat flow, which is specific to a deposit of molten material on a solid substrate. Laves phases formed in the mixing zone between the laser-deposited layers and the GCI substrate, in the form of small light-colored islands precipitated interdendritically (Fig. 4c). The distribution of the chemical elements along a line that crosses the interface between the laser deposited layer of IN718 and the substrate of GCI is shown in Fig. 4d. A mixing zone of ~ 200 microns wide is formed at the interface, where an obvious decrease of Ni and Cr concentrations can be observed.

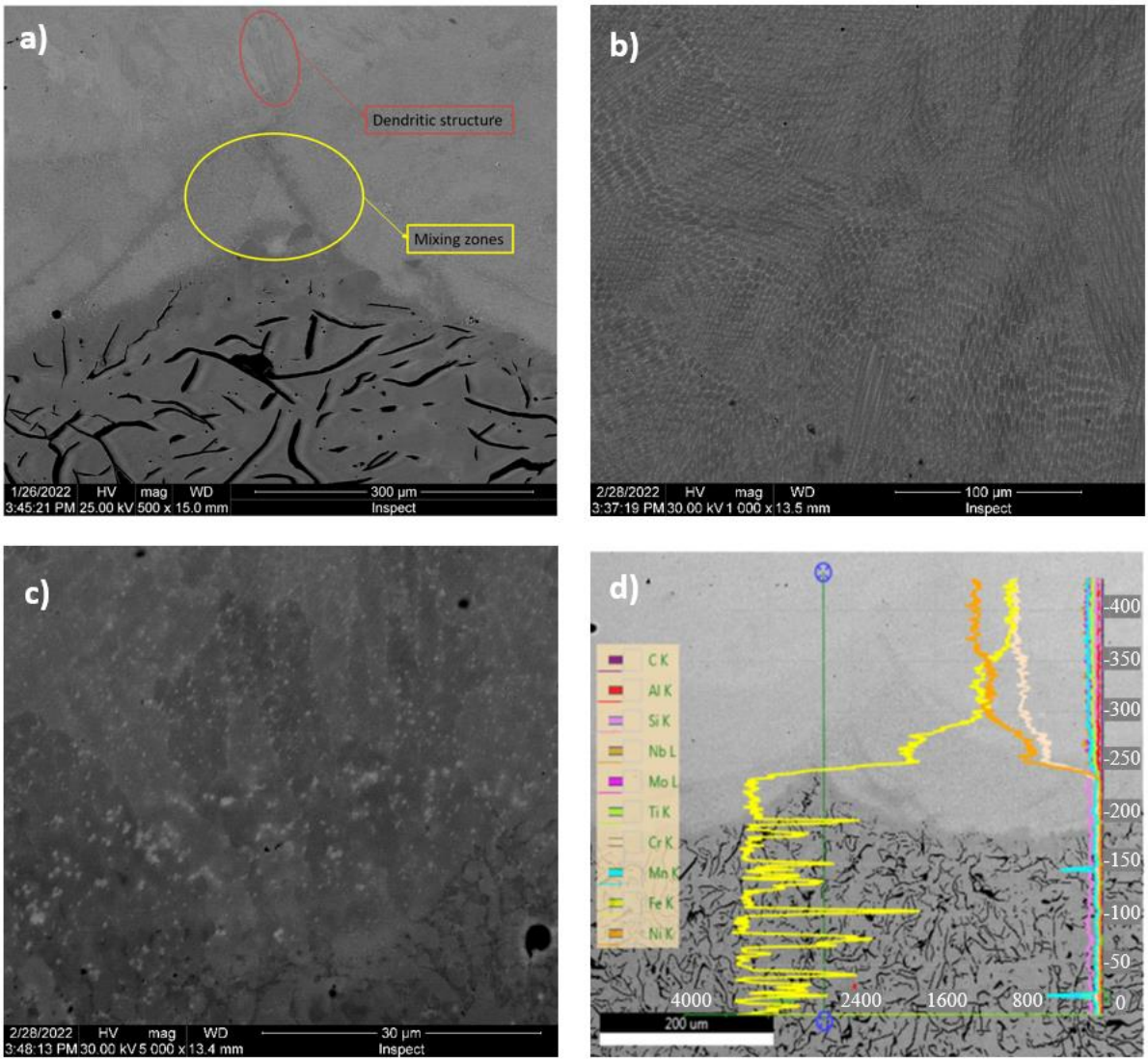

Fig. 4 SEM images of cross sections zones through laser deposition layers. transition zone between two layers of IN718 Laser deposition and GCI substrate (a); cellular dendritic grains of In718 laser deposition (b); detail of mixing zone highlighting the Laves phases location (c); line scan through interface of laser clad on transverse direction (d)

Compositional analyze

An interesting aspect was noticed at the intersection and overlap areas of the successive layers deposited with laser (Figure 5). It can be seen how the first layer deposited with the IN718 alloy suffered the most important dilution effect with the GCI substrate, while for the subsequent successive layers (layer 2 and layer 3) the dilution decreased. Ni and Cr are the elements with the lowest diffusion tendency in GCI.

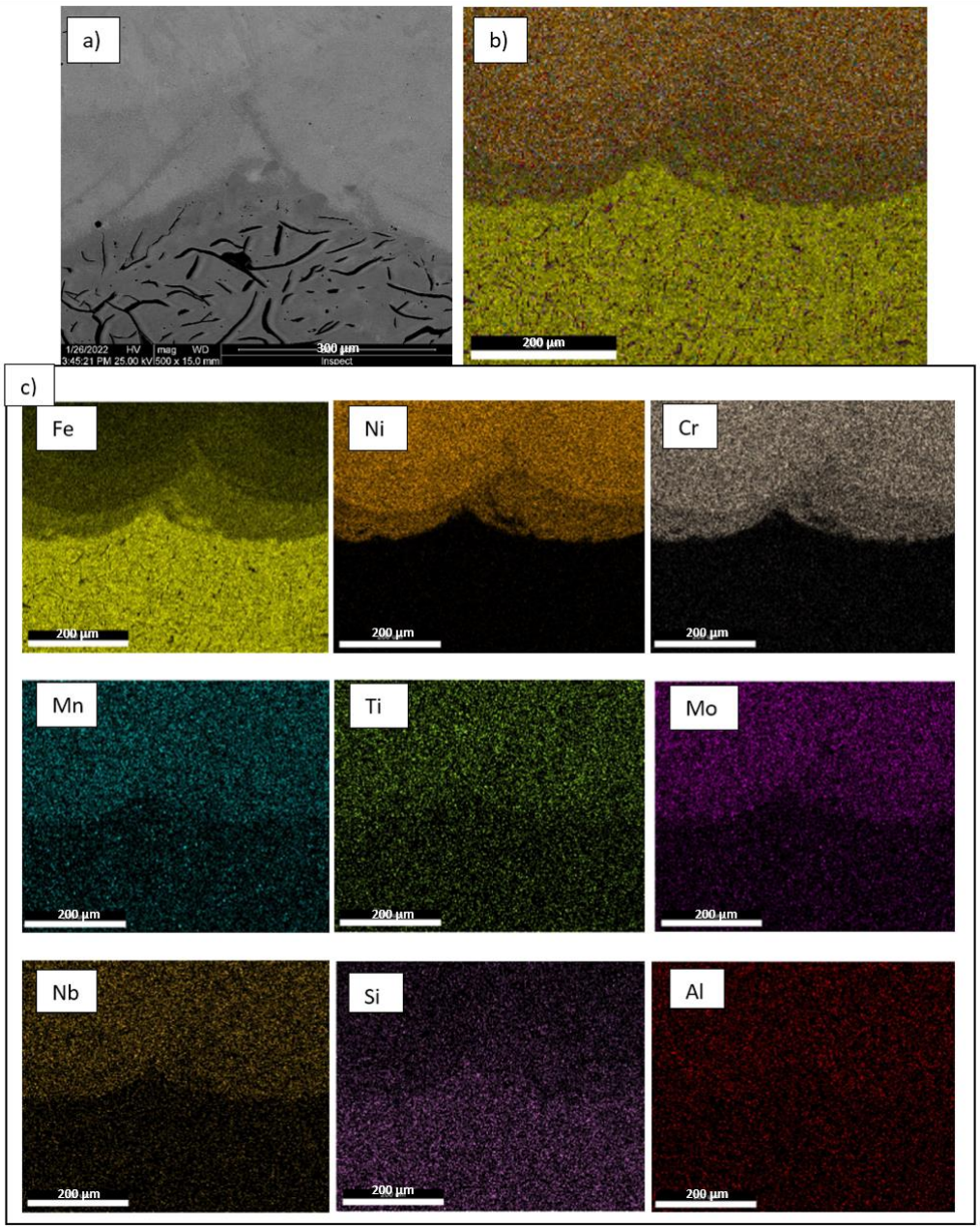

Fig. 5 Chemical elements distribution on transverse cross section of laser deposited layers SEM image of analyzed area (a); EDS global image (b); EDS elements distribution maps. Magnification bar 200 µm (c)

For the quantitative highlighting of the dilution effects at the interface between the two materials, EDS spot analyzes were performed in different areas: on the layer 1 and 2 of IN718 deposition, at the interface with the GCI substrate, in the cast iron at approx. 25 µm below the interface, on the mixing zone at intersection between layers 1 and 2, on the carbon-rich areas situated on the interface with the GCI substrate (Fig. 6).

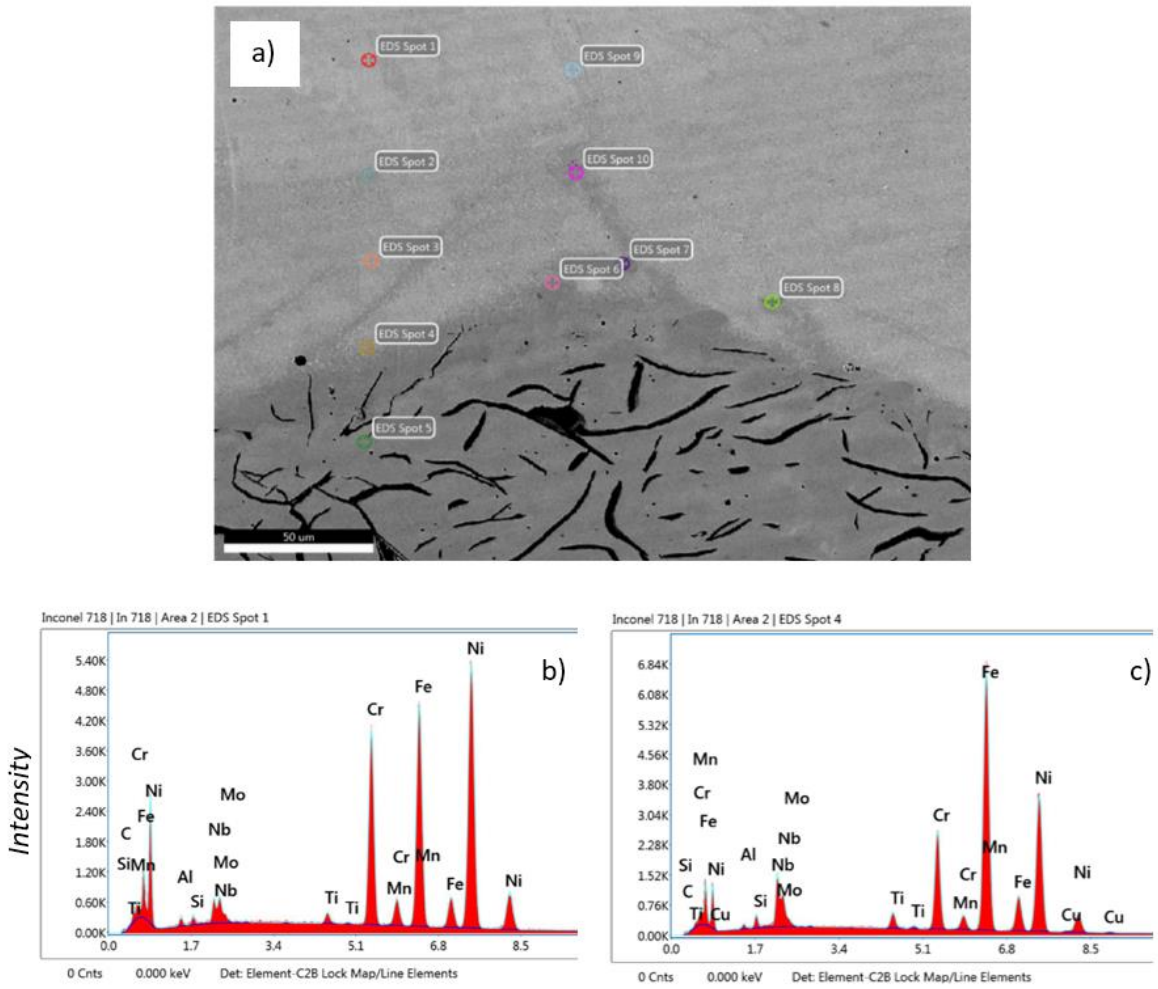

Fig 6. EDS spot analyzes around the interface zone. SEM image with the spot analyzes loccation (a); elements spectrum for EDS spot 1 (b); elements spectrum for EDS spot 4 (c).

EDS measuring points (spots 9 and 10) are placed in the mixing zone between GCI and IN718 deposited layer, while spots 4, 6, 7 and 8 are situated on the interface between clad and the GCI substrate. The chemical composition for each EDS measurement point is shown in table 4. Small amounts of Cu (of 0.47wt% to 0.58wt %) from GCI are present in the EDS analysis, but were not taken into account in Table 4.

According to EDS chemical analysis data, the Ni concentration decreased from the standard values of 52.8 wt% (according to the spectral chemical analysis on powder material IN718, Table 1) to less than 31 wt % at the interface with the GCI substrate, and the iron content increases as mixing effect of the two materials. The variation of Ni concentration in different points of the cross-sections is due to dilution effect. The maximum dilution effect occurs in the first layer of IN718 deposited on the gray cast iron substrate (about 31.33 wt% Ni). For the second layer, dilution is lower, and the Ni content reaches 45.86 wt% (spot 1). For the next layers (3 and 4) the Ni concentration reaches the nominal value specified in the powder quality certificate. Below the GCI substrate separation line, the Ni concentration reaches about 0.1 wt%, indicating the lack of diffusion effect of this element in the substrate.

A similar evolution can be observed in case of Cr, whose concentration decreased from 19.2 wt% in standard composition (Table 1) to 18.09 wt% in second laser-coated layer and then to 15.68 wt% in the first laser-clad layer. Small quantities of Cr have been detected bellow the interface with the substrate (0.29 to 0.83 wt%).

Other chemical elements from IN718 alloy, such as Nb, Mo, Ti and Al, have a decrease in chemical concentration as they approach the substrate interface. However, on the interface area (Spot 4, Table 4), an increase in the concentration of Nb (7.23 wt%) has been obtained, due to the formation of Laves phases or carbides [36]. No fragile compounds and no cracking effects have been detected at the clad interface with the GCI substrate.

Table 4. Chemical composition of EDS spot analyzes for Fig. 9[wt%]

EDS spot	Ni	Cr	Nb	Mo	Ti	Al	Si	Mn	C	Fe
1	45.86	18.09	2.68	2.00	0.79	0.88	0.63	0.52	0.63	
2	37.22	14.24	0.85	1.38	0.33	0.79	0.91	0.37	0.50	
3	36.28	15.68	1.08	1.79	0.46	0.81	1.16	0.47	0.46	
4	31.33	11.83	7.23	2.29	1.50	0.55	1.00	0.35	0.73	
5(GCI)	0.10	0.29	0.20	0.22	0.17	0.57	2.48	0.47	0.73	balance
6	-	0.83	-	-	-	0.54	2.25	-	081	
7	1.27	1.56	-	-	-	-	2.42	0.46	0.80	
8	0.34	1.34	-	-	-	-	2.46	-	0.81	
9	45.31	18.34	3.56	2.24	1.07	0.99	0.61	0.35	0.62	
10	14.64	5.87	0.28	0.56	0.25	0.58	1.56	0.35	0.65	

In the mixing zone of the overlap molten layers (Spot 10, Fig. 9a), a decrease of Ni and Cr concentration was observed, together with an increase of Fe concentration (75.26 wt%). This evolution is due to mixing effects between the layers during DED. When the first laser layer is deposited, the IN718 powder and a surface layer of GCI are melted together. Some of the alloying elements from IN718, like Cr, Nb and Ti form carbides and Laves phase. The convection currents from the molten metal allow carbon from GCI to rapidly react with the high carbon affinity elements (Cr, Nb, Ti) from IN718, in the interface area. The carbon atoms cannot diffuse too much into the deposited metal, this phenomenon being limited by the low diffusion coefficient of C in the Ni-rich alloy and by the short interaction time with the laser beam.

In carbon rich (2-6.67wt%) Fe alloys such as GCI, this element is found either free (nodular graphite, lamellar, stellate, vermicular) or in cementite or ledeburite. Marangoni convection model can be used to explain the mechanism of carbon migration from the graphite lamella trough the melt pool and scattered in the deposited structure, close to the interface. During the DED process, the recorded temperature of melt pool was constant ~1450˚C. Due to rapid heating-cooling cycles, the C structures can coalesce and migrate from the GCI in the deposited structure and be trapped inside the new layer during solidification. A schematic representation of this mechanism is presented in figure 2. However, we demonstrated that using the optimal process parameters the free carbon accumulation in the deposited layer can be almost completely ruled out.

Hardness

Sets of ten measurements were performed in 6 different of each sample in order to achieve an accurate value of the deposited material's hardness. The average hardness of GCI in a commercial brake disc was of 290 ± 9 HV, while the hardness of the IN718 deposited material,

conducted on the polished surface of the deposited layer, showed a 430 ± 16 HV value, which is higher by ~50%, as compared to the substrate. It must be mentioned that tests were performed in various locations of the coated samples and on multiple samples, indicating a homogeneous hardness of the coating. The values for casted IN718 commercially available alloys are ≤380 HV [37]. In case of Selective Laser Melting (SLM) lower microhardness values of around 281±18 HV [38] or 330-390 HV [39, 40] were reported. For DED, the hardness increase by 10% as compared to the highest reported values in case of SLM or casted samples could be due to the high Nb content close to the surface. It is known that the increase of the Nb content favors the formation of hard phases in Inconel alloys [41, 42]. Nb is soluble in the Ni based austenite and it strengthens it by producing both an elastic stress caused by the atomic size difference and an internal stress by the difference of elasticity modulus between austenite and Nb atoms [43, 44] From Table 4, one can see that closer to the surface the Nb content is of ~3 w.t.%, while in the vicinity of the interface with the GCI substrate, it was not detected by EDS.

Tribological properties

The wear resistance of GCI substrate and IN718 deposited layers was tested at room temperature under dry sliding conditions and the friction coefficients evolution is shown in Fig. 7. The IN718 surface presents a superior wear resistance compared to the substrate specimen at the same wear parameter conditions. The coefficient of friction (CoF) between the round head of Steel 440C stylus and the GCI substrate was of 0.53 with the tendency to decrease after 200 s of continuous testing. This is a sign that the surface was leveled by the stylus and became smoother after repeated passages over the same area. Oppositely, the IN718 coatings displayed a 0.12 higher CoF vs the 440C pin, as compared with the substrate specimens. In this case, the COF was not affected by the repeated interaction between the pin and the coating over the 300 s testing interval, which was indicative of a higher hardness. The pin had not succeeded to induce a smoothening of the surface after repeated passage over the same surface in the testing interval.

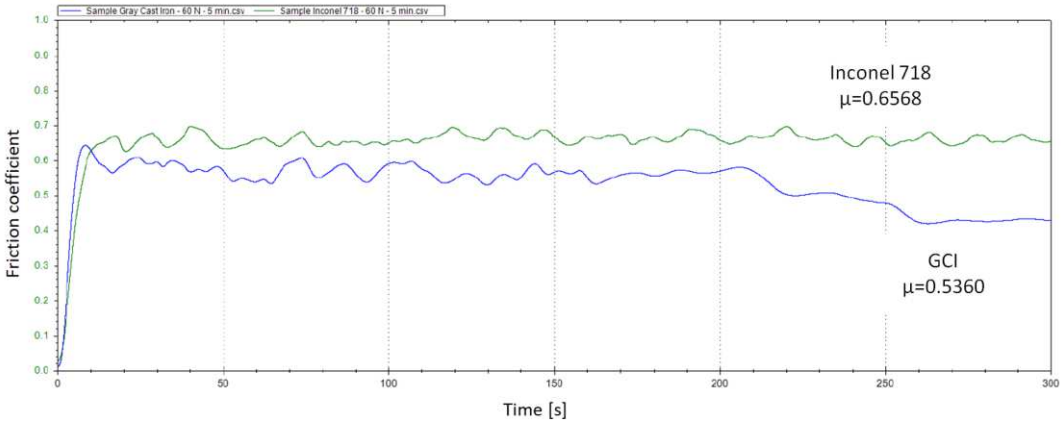

Fig. 7 Coefficient of Friction in case of GCI and Inconel 718 registered in the circular motion

The wear tests performed on the GCI substrate and Inconel 718 superalloy specimens were finalized with an inspection of the worn areas via three-dimensional mapping with a confocal microscope. The 3D morphology and cross–section profile of the wear tracks are shown in Fig. 8. The circular wear reciprocating test showed significant tribological differences between the uncoated and Inconel 718 coated samples, tested at room temperature. Fig. 8a reveals a low value of the wear track depth for the IN718 deposited layers (-50 μm), while the wear track depth of the GCI uncoated substrate (Fig. 8b) was 3 times higher (-150 μm) than the one of the samples coated with IN718.

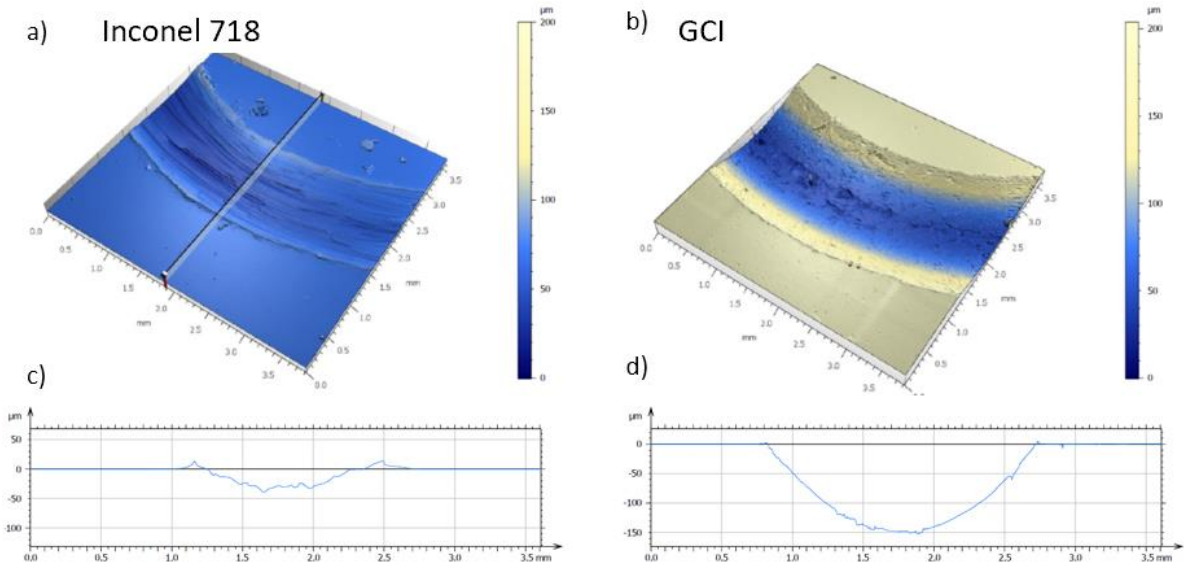

Fig. 8 Graphical representation of wear track depth (a) and a selected section (b) of the IN718 vs GCI surfaces

Corrosion properties

It is expected that the IN718 layer to have superior corrosion properties to GCI substrates, as the IN718 is mainly a Ni-Cr alloy, both elements being known for their ability to form a natural oxide protective layer against corrosion. The following tests aim to show the magnitude of the IN718 corrosion protection superiority as compared to GCI. The corrosion tests were conducted in 3,5% NaCl aqueous solution. Fig. 9a shows the variation of the open circuit potential (EOC), while Fig. 9b presents the potentiodynamic polarization Tafel curves for the investigated samples. From the Tafel curve, the corrosion potential (E_{corr}), corrosion current density (i_{corr}), the slope of the anodic (βa) and cathode (βc) curve of the tested materials were determined. The values of the corrosion parameters of the tested materials are listed in Table 4.

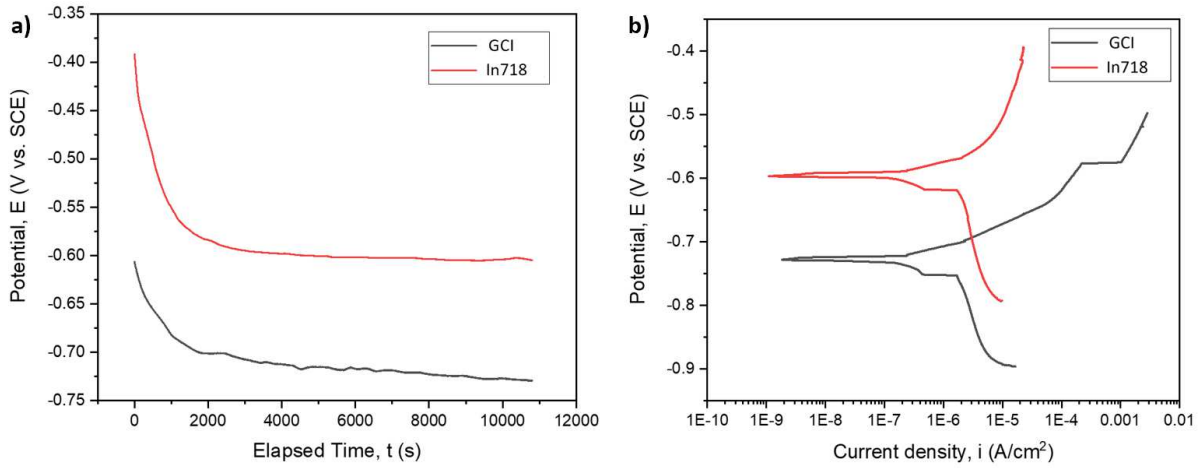

Fig. 9 The open circuit potential evolution (a) and the potentiodynamic polarization Tafel curves (b) of the IN718 deposited layers and the GCI substrate.

It can be observed (Figure 9b and Table 5) that E_{corr} of the IN718 deposited layers is significantly higher than the GCI substrate. The higher the corrosion potential of the material, the lower the corrosion current, resulting in a superior corrosion resistance. Also, a smaller value of the corrosion current density (i_{corr}) indicates a better corrosion resistance and it validates once again that the IN718 deposited layers protect the brake disc from corrosion.

Table 5 Corrosion parameters of GCI substrate and IN718 deposited layers by DED

Sample	E_{oc} (mV)	E_{corr} (mV)	i_{corr} (µA/cm²)	β_c (mV)	β_a (mV)
GCI	-729	-760	3.925	237.21	59.82
IN718	-604	-597	1.501	98.91	103.08

Based on the parameters presented in table 5, we can calculate the polarization resistance according to ASTM G59-97 (2014) standard, given by the equation:

$$R_p = \frac{1}{2.303} \frac{\beta_a|\beta_c|}{\beta_a+|\beta_c|} \frac{1}{i_{corr}} \quad (2)$$

where,
R_p is the polarization resistance;
β_a is the slope of the anodic curve of the tested materials
β_c is the slope of the cathode curve of the tested materials
i_{corr} is the corrosion current density
The polarization resistance is defined as the resistance of a sample to corrosion during the application of an external current.
The way to calculate the corrosion rate (CR) based on the i_{corr} [45], which is recommended by ASTM G102-89 [46] is shown in equation (3):

$$CR\ (\frac{mm}{year}) = \frac{i_{corr} \times k_1 \times EW_{Metal}}{\rho} \quad (3)$$

where,
k_1 is a constant that defines the units for the corrosion rate and its value is 3272 mm/(A cm year)
EW_{Metal} is the equivalent weight in grams, which for metallic compounds is 27.92
ρ is density, which for GCI is ~7 g/cm³ and for IN718 is 8.12 g/cm³

The resulted values of polarization resistance (R_p) and corrosion rate (CR) are presented in table 6 for both investigated materials, IN718 deposited by DED and the GCI substrate.

Table 6 Polarization resistance and corrosion rate of GCI substrate and Inconel 718 deposited layers

Sample	Rp (kΩxcm²)	CR (mm/year)
GCI	5,29	0.05
IN718	22,20	0.01

It was found that the surface coated with IN718 by DED increased by four times the polarization resistance of the electrode. This information is validated by the corrosion rate of the GCI, which is three times lower than the CR of the IN718 deposited layers, in 3.5 wt.% NaCl aqueous solution.

Functional tests

Once the IN718 deposited layers demonstrated to have improved mechanical properties, the optimal parameters were used to fully coat two brake discs by DED (fig. 10a). After deposition, a post-processing step by turning machining (fig. 10b) was inherent in order to achieve the dimensions specified in the technical drawing.

Brake discs coated by DED with IN718 layers and post machined by turning were tested for measuring the braking force on a roller brake tester at an authorized car service. The discs were mounted on a Renault Megane and tested for conformity with the national legislation for vehicles circulation (Fig. 10c).

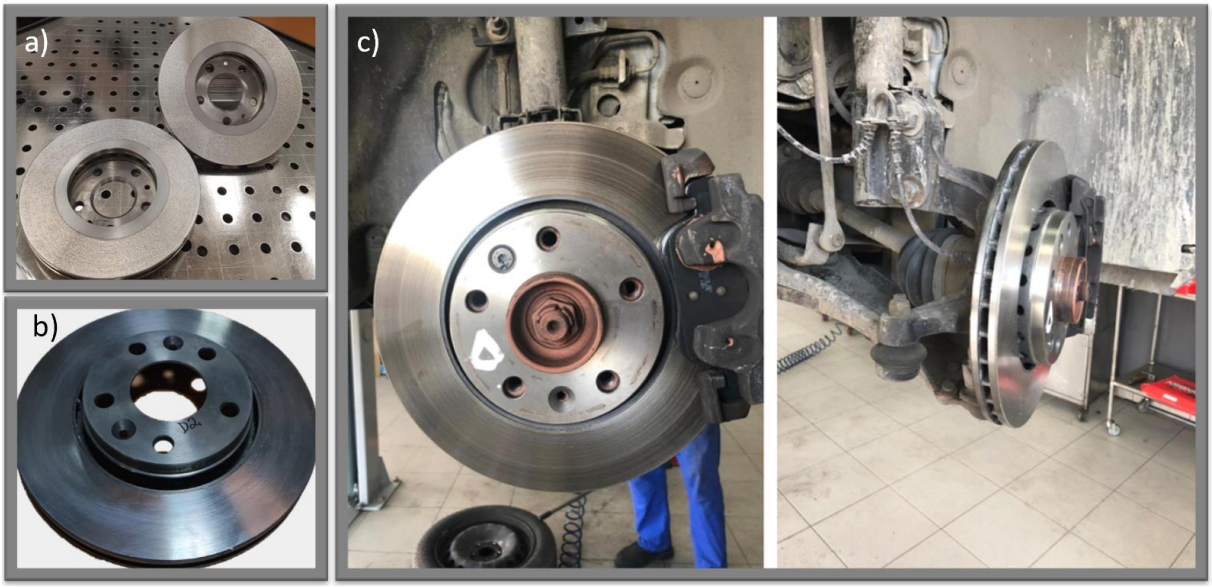

Fig. 10 Brake discs coated by DED with IN718 (a); final product post machining (b) and functionally tested on a vehicle in an authorized car service unit(c)

The friction force was the interest parameter for these tests. The friction force is calculated using Eq. 4:

$$F_f = c_f \times F_p , \tag{4}$$

where,
F_f is the friction force; c_f is the friction coefficient; F_p is the pressing force of the brake pad

The test results showed a value of ~2700 N.
The friction coefficient is calculated based on Eq. 5:

$$c_f = \frac{\sum_{i=1}^{n} F_{is} + F_{id}}{G} \times 100(\%) , \tag{5}$$

where,
F_{is} (daN) – braking force on the left wheel on the left side of the front axel i;
F_{id} (daN) – the braking force on the right wheel on the right side of the front axel i;
n – number of front axels;
G (daN) – weight of the vehicle.

The friction coefficient value for the DED IN718 coated brake discs was of 71. We mention that the critical value over which a braking system of a vehicle is considered reliable is of 58, according to the legal regulations for circulation of vehicles on public roads [43].

Overall, the braking system consisting of the brake disc and brake pad fulfilled the testing standards for vehicles imposed by European regulations and received a conformity certificate.

4. Conclusions

In this paper, the properties of a IN718 metallic deposited layers obtained by Direct Energy Deposition laser method on GCI substrates were analyzed. The coating material IN718 alloy was initially in form of spherical powder, which was guided by three-beam nozzle and melted by the laser beam, obtaining an adherent, compact and uniform layer after solidification, on the surface of the GCI substrate.

The results reveal improved mechanical properties of GCI coated with IN718 by DED and the following conclusions can be drawn:

- The interface between substrate and the deposited material was uniform, forming a compact bonding of the two materials. The 40% overlap ratio was selected as the optimal value in order to achieve a homogenous, crack and pores-free surface in the alloyed region. The diffusion of main chemical elements (Ni, Cr, Nb, Ti) from IN718 laser deposited layers on the GCI substrate was negligible and no fragile compound that can produce cracks has been detected at the interface.
- The average hardness of GCI is 290 ± 9 HV, while the hardness of the IN718 deposited material was of 430 ± 16 HV value, which is ~50% higher.
- The GCI substrate had a friction coefficient (CoF) of 0.5 and dropped to 0.4 during testing because of the surface leveling following multiple passes of the pin over the same area, while the IN718 coatings presented CoF higher by 0.12 as compared to the substrate material and were not affected significantly by erosion during testing. The depth of the wear track for the layers deposited with IN718 was -50 µm, while the depth of the wear track of the exposed substrate GCI was 3 times higher (-150 µm). IN718 succeeded to protect the substrate against wear, which translates into an extension of the brake disc lifetime.
- The corrosion resistance of the coating was superior to that of the GCI substrate in 3.5 wt.% NaCl aqueous solution. It was found that the surface coated with IN718 by DED method increased by four times the polarization resistance of the electrode and displayed a 40% smaller value of the corrosion current density (i_{corr}), which indicates a better corrosion resistance.
- The couple between the coated brake discs and the brake pads was tested by measuring the braking force and the friction coefficient in real environment in an authorized car testing facility. They fulfilled the testing standards for vehicles imposed by European regulations and received a conformity certificate.

The brake disc coating with a hard and highly resistant to corrosion alloy could be an interesting solution for the vehicles wheels engineering. The cost is kept low, as the main part of the disc is made of inexpensive GCI, while the deposited layer adds a prolonged lifetime of the part and reduces pollution caused by metal particles expelled in the atmosphere during braking.

Author Contributions: Conceptualization, D.C. and I.V; methodology, D.C., I.V., A.C.P.; software analysis, S.M; validation, D.C. and I.V.; formal analysis, A.C.P and C.C.; investigation, D.C., A.C.P., I.V. and C.C; resources, I.V., A.C.P.; data collection, D.C and I.V.; writing- original draft preparation, D.C., S.M., C.C, I.V. and A.C.P; writing-review and editing, D.C and I.V.; supervision, A.C.P. and I.V. All authors have read and agreed to the published version of the manuscript.

Institutional Review Board Statement: Not applicable.

Informed Consent Statement: Not applicable.

Data Availability Statement: The data and all related information presented in this study are available on request from the corresponding authors.

Acknowledgments: This research study has been conducted in the framework of POC-G, contract no. 135/2016, and UEFISCDI 45/2021. This work was also supported by grants from the Romanian Ministry of Education and Research, CNCS-UEFISCDI, project numbers PN-

III-P4-ID-PCE-2020-1634 and PN-III-P2-2-1-PED-2019-3953, within PNCDI III, and the Romanian Ministry of Education and Research under the Romanian National Nucleu Program LAPLAS VI, contract no. 16N/2019.

The authors would like to thank Rtec-Instruments Romanian representatives for their valuable help with hardness and tribological testing of the samples.

Conflicts of Interest: The authors declare no conflict of interest.

Bibliography

1. Rashid A (2014) Overview of Disc Brakes and Related Phenomena-a review. Int J Veh Noise Vib 10:301. https://doi.org/10.1504/IJVNV.2014.065634
2. Thornton R, Slatter T, Jones AH, Lewis R (2011) The effects of cryogenic processing on the wear resistance of grey cast iron brake discs. Wear 271:2386–2395. https://doi.org/10.1016/J.WEAR.2010.12.014
3. Lu S, Zhou J, Wang L, Liang J (2021) Influence of MoSi2 on the microstructure and elevated-temperature wear properties of Inconel 718 coating fabricated by laser cladding. Surf Coatings Technol 424:127665. https://doi.org/10.1016/J.SURFCOAT.2021.127665
4. Roubicek V, Raclavska H, Juchelkova D, Filip P (2008) Wear and environmental aspects of composite materials for automotive braking industry. Wear 265:167–175. https://doi.org/10.1016/J.WEAR.2007.09.006
5. Grigoratos T, Martini G (2015) Brake wear particle emissions: a review. Environ Sci Pollut Res 22:2491–2504. https://doi.org/10.1007/S11356-014-3696-8/TABLES/5
6. Nogueira APG, Carlevaris D, Menapace C, Straffelini G (2020) Tribological and Emission Behavior of Novel Friction Materials. Atmos 2020, Vol 11, Page 1050 11:1050. https://doi.org/10.3390/ATMOS11101050
7. Dizdar S, Lyu Y, Lampa C, Olofsson U (2020) Grey Cast Iron Brake Discs Laser Cladded with Nickel-Tungsten Carbide—Friction, Wear and Airborne Wear Particle Emission. Atmos 2020, Vol 11, Page 621 11:621. https://doi.org/10.3390/ATMOS11060621
8. Tonolini P, Montesano L, Pola A, et al (2021) The effect of laser-cladding on the wear behavior of gray cast iron brake disc. Procedia Struct Integr 33:1152–1161. https://doi.org/10.1016/J.PROSTR.2021.10.129
9. The Welding Institute (2019) What is Extreme High Speed Laser Application (EHLA)? In: Tech. Knowl. https://www.twi-global.com/technical-knowledge/faqs/what-is-ehla. Accessed 21 Jan 2022
10. Li T, Zhang L, Bultel GGP, et al (2019) Extreme High-Speed Laser Material Deposition (EHLA) of AISI 4340 Steel. Coatings 2019, Vol 9, Page 778 9:778. https://doi.org/10.3390/COATINGS9120778
11. Zhu L, Liu Y, Li Z, et al (2020) Microstructure and properties of Cu-Ti-Ni composite coatings on gray cast iron fabricated by laser cladding. Opt Laser Technol 122:105879. https://doi.org/10.1016/j.optlastec.2019.105879
12. Wang T, Wang C, Li J, et al (2021) Microstructure and wear properties of laser-clad NiCo alloy coating on Inconel 718 alloy. J Alloys Compd 879:160412. https://doi.org/10.1016/J.JALLCOM.2021.160412
13. Zhu L, Yang Z, Xin B, et al (2021) Microstructure and mechanical properties of parts formed by ultrasonic vibration-assisted laser cladding of Inconel 718. Surf Coatings Technol 410:126964. https://doi.org/10.1016/J.SURFCOAT.2021.126964
14. Thawari N, Gullipalli C, Katiyar JK, Gupta TVK (2021) Effect of multi-layer laser cladding of Stellite 6 and Inconel 718 materials on clad geometry, microstructure evolution and mechanical properties. Mater Today Commun 28:102604.

https://doi.org/10.1016/J.MTCOMM.2021.102604
15. Cui C, Wu M, Miao X, et al (2021) The effect of laser energy density on the geometric characteristics, microstructure and corrosion resistance of Co-based coatings by laser cladding. J Mater Res Technol 15:2405–2418. https://doi.org/10.1016/J.JMRT.2021.09.073
16. Zhong C, Gasser A, Kittel J, et al (2016) Improvement of material performance of Inconel 718 formed by high deposition-rate laser metal deposition. Mater Des 98:128–134. https://doi.org/10.1016/J.MATDES.2016.03.006
17. Li Y, Dong S, Liu X, et al (2021) Interface phase evolution during laser cladding of Ni-Cu alloy on nodular cast iron by powder pre-placed method. Opt Laser Technol 135:106684. https://doi.org/10.1016/J.OPTLASTEC.2020.106684
18. Yi P, Zhan X, He Q, et al (2019) Influence of laser parameters on graphite morphology in the bonding zone and process optimization in gray cast iron laser cladding. Opt Laser Technol 109:480–487. https://doi.org/10.1016/J.OPTLASTEC.2018.08.028
19. Olofsson U, Lyu Y, Åström AH, et al (2021) Laser Cladding Treatment for Refurbishing Disc Brake Rotors: Environmental and Tribological Analysis. Tribol Lett 69:1–11. https://doi.org/10.1007/S11249-021-01421-1/TABLES/6
20. Liu Y, Zhan X, Yi P, et al (2018) Research on the transformation mechanism of graphite phase and microstructure in the heated region of gray cast iron by laser cladding. Opt Laser Technol 100:79–86. https://doi.org/10.1016/J.OPTLASTEC.2017.09.051
21. Zhang T, Li P, Zhou J, et al (2021) Microstructure evolution of laser cladding Inconel 718 assisted hybrid ultrasonic-electromagnetic field. Mater Lett 289:129401. https://doi.org/10.1016/J.MATLET.2021.129401
22. Ocelík V, Oliveira U De, Boer M De, Hosson JTM De (2007) Thick Co-based coating on cast iron by side laser cladding : Analysis of processing conditions and coating properties. 201:5875–5883. https://doi.org/10.1016/j.surfcoat.2006.10.044
23. Fernández E, Cadenas M, González R, et al (2005) Wear behaviour of laser clad NiCrBSi coating. Wear 259:870–875. https://doi.org/10.1016/J.WEAR.2005.02.063
24. McLouth TD, Bean GE, Witkin DB, et al (2018) The effect of laser focus shift on microstructural variation of Inconel 718 produced by selective laser melting. Mater Des 149:205–213. https://doi.org/10.1016/J.MATDES.2018.04.019
25. Huang K, Li W, Pan K, et al (2021) Microstructure and Corrosion Properties of La2Zr2O7/NiCoAlY Thermal Barrier Coatings Deposited on Inconel 718 Superalloy by Laser Cladding. Coatings 2021, Vol 11, Page 101 11:101. https://doi.org/10.3390/COATINGS11010101
26. Stanciu EM, Pascu A, Ţierean MH, et al (2016) Dual Coating Laser Cladding of NiCrBSi and Inconel 718. Mater Manuf Process 31:1556–1564. https://doi.org/10.1080/10426914.2015.1103866
27. Zhang H, Zou Y, Zou Z, Zhao W (2015) Comparative study on continuous and pulsed wave fiber laser cladding in-situ titanium-vanadium carbides reinforced Fe-based composite layer. Mater Lett 139:255–257. https://doi.org/10.1016/J.MATLET.2014.10.102
28. Lee HK (2008) Effects of the cladding parameters on the deposition efficiency in pulsed Nd:YAG laser cladding. J Mater Process Technol 202:321–327. https://doi.org/10.1016/J.JMATPROTEC.2007.09.024
29. Pinkerton AJ, Li L (2003) An investigation of the effect of pulse frequency in laser multiple-layer cladding of stainless steel. Appl Surf Sci 208–209:405–410. https://doi.org/10.1016/S0169-4332(02)01420-4
30. Li Y, Dong S, Yan S, et al (2019) Elimination of voids by laser remelting during laser cladding Ni based alloy on gray cast iron. Opt Laser Technol 112:30–38. https://doi.org/10.1016/j.optlastec.2018.10.055
31. Li W, Yang X, Xiao J, Hou Q (2021) Effect of WC mass fraction on the microstructure

and friction properties of WC/Ni60 laser cladding layer of brake discs. Ceram Int 47:28754–28763. https://doi.org/10.1016/J.CERAMINT.2021.07.035
32. Xin B, Ren J, Wang X, et al (2020) Effect of Laser Remelting on Cladding Layer of Inconel 718 Superalloy Formed by Laser Metal Deposition. Mater 2020, Vol 13, Page 4927 13:4927. https://doi.org/10.3390/MA13214927
33. Mazzucato F, Forni D, Valente A, Cadoni E (2021) Laser Metal Deposition of Inconel 718 Alloy and As-built Mechanical Properties Compared to Casting. Mater 2021, Vol 14, Page 437 14:437. https://doi.org/10.3390/MA14020437
34. Fan H-Y, Tu-Nan - R, Gusev DS, Lyukhter AB (2017) Influence of technological parameters on the geometry of single-track laser clad nickel based alloy on grey cast iron substrate. J Phys Conf Ser 941:012037. https://doi.org/10.1088/1742-6596/941/1/012037
35. Liu P, Sun S-Y, Xu S-B, et al (2018) Effect of Solid Solution + Double Ageing on Microstructure and Properties in the Layer by Layer of the Z-Y Interface of Inconel 718 alloys Fabricated by SLM. Mater Res 21:20180395. https://doi.org/10.1590/1980-5373-MR-2018-0395
36. Zhang YN, Cao X, Wanjara P (2013) Microstructure and hardness of fiber laser deposited Inconel 718 using filler wire. Int J Adv Manuf Technol 69:2569–2581. https://doi.org/10.1007/S00170-013-5171-Y
37. Inconel 718 from China manufacturer - Taixin Steel Co., Limited. http://www.alloyss.com/inconel-718.html. Accessed 23 Feb 2022
38. Jiang R, Mostafaei A, Pauza J, et al (2019) Varied heat treatments and properties of laser powder bed printed Inconel 718. Mater Sci Eng A 755:170–180. https://doi.org/10.1016/J.MSEA.2019.03.103
39. Zhang Y, Li Z, Nie P, Wu Y (2013) Effect of cooling rate on the microstructure of laser-remelted INCONEL 718 coating. Metall Mater Trans A Phys Metall Mater Sci 44:5513–5521. https://doi.org/10.1007/S11661-013-1903-8/TABLES/4
40. Yang H, Yang J, Huang W, et al (2018) The printability, microstructure, crystallographic features and microhardness of selective laser melted Inconel 718 thin wall. Mater Des 156:407–418. https://doi.org/10.1016/J.MATDES.2018.07.007
41. Liu H, Guo K, Sun J, Shi H (2022) Effect of Nb addition on the microstructure and mechanical properties of Inconel 718 fabricated by laser directed energy deposition. Mater Charact 183:111601. https://doi.org/10.1016/J.MATCHAR.2021.111601
42. Wang J, Wang Y, Su Y, Shi J (2022) Evaluation of in-situ alloyed Inconel 625 from elemental powders by laser directed energy deposition. Mater Sci Eng A 830:142296. https://doi.org/10.1016/J.MSEA.2021.142296
43. Regulation No 90 of the Economic Commission for Europe of the United Nations (UN/ECE). http://www.unece.org/trans/main/wp29/wp29wgs/wp29gen/wp29fdocstts.html. Accessed 25 Feb 2021
44. E/ECE/324/Rev.1/Add.89/Rev.3/Amend.6−E/ECE/TRANS/505/Rev.1/Add.89/Rev.... | Law Insider. https://www.lawinsider.com/contracts/cHc1b10g1jm. Accessed 23 Feb 2022
45. Quej-Ake LM, Contreras A, Aburto J (2018) The effect of non-ionic surfactant on the internal corrosion for X52 steel in extra-heavy crude oil-in-water emulsions. Anti-Corrosion Methods Mater 65:234–248. https://doi.org/10.1108/ACMM-03-2017-1770/FULL/XML
46. Astm (1999) Standard Practice for Calculation of Corrosion Rates and Related Information. Astm G 102 89:1–7. https://doi.org/10.1520/G0102-89R10